Glass Transition Behavior of Clay Aerogel/Poly(vinyl alcohol) Composites

Suneel Bandi and David A. Schiraldi*

Department of Macromolecular Science and Engineering, Case Western Reserve University, Cleveland, Ohio 44106-7202

Received May 26, 2006; Revised Manuscript Received July 11, 2006

ABSTRACT: In polymer/clay nanocomposites, the size and morphology of the dispersed clay are crucial in determining the macroscopic composite properties. Clay can be converted into an aerogel structure through a freeze-drying process which results in a reduction of its density from 2.35 to 0.05 g/cm^3. The morphology of these clay aerogels resembles a house of cards structure. Low weight fraction (0.5−4 wt %) composites of clay and clay aerogel with a poly(vinyl alcohol) (PVOH) matrix polymer were prepared. Glass transition temperature (T_g) behaviors of clay/PVOH composites were investigated as a function of size, loading, and dispersion of clay and clay aerogel in the polymer matrix. The trends in T_g measured from both dynamic mechanical analysis and differential scanning calorimetry are similar, exhibiting a maximum value at 1 wt % loading for both clay and clay aerogel and then decreasing with additional filler content. Although the trends are similar, the drop in T_g at 4 wt % clay composite is considerably larger than that for a similar loading of clay aerogel. In comparison with the mesoscale clay aerogel, the nanoscale clay shows better dispersion and higher interfacial interaction with the polymer, which enhances polymer crystallinity at lower weight fractions and increases polymer free volumes at higher weight fractions. The relative changes in T_g are proposed to be the result of two competing effects: (i) surface interaction which strengthens the interface (decreasing chain mobility) and (ii) enhanced interfacial free volume due to the lower bulk crystallinity of polymer chains (increasing chain mobility).

Introduction

Smectite silicates, such as montmorillonite clay, possess charged, high aspect layered structures and are well-known for their ability to reinforce polymers.[1] Montmorillonite and similar clays form gels in water via hydration of the cationic layers present within their 2:1 phyllosilicate structures.[1] When freeze-dried, smectite clay/water gels produce "house of cards"-like aerogel structures, materials with bulk densities in the 0.01−0.1 g/cm^3 range. These low-density aerogel structures are obtained through volume expansion and alignment/shearing of high-density clay platelets. Freeze-drying of the gels has two effects: (1) maintenance of the gel structure (face to edge conformation) and (2) enhancement of the clay aspect ratio by shear alignment of the clay gels between growing ice fronts and on the ice crystal faces.[2−8] Room temperature drying of clay gel is incapable of forming such aerogel structures. The approach of preconverting clay into an aerogel and then combining it with polymers to produce composite materials is appealing in its simplicity, its ability to be adapted to a wide range of polymeric matrixes, and from the absence of thermodynamic and kinetic barriers present when more traditional expanded/exfoliated clay fillers are dispersed in polymer matrixes.[9]

Clay composites which incorporate hydrophilic organic polymers exhibit enhanced interfacial interactions through hydrogen bonding as polymer molecules are adsorbed on the clay surface. Poly(vinyl alcohol) (PVOH) and poly(ethylene oxide) (PEO) have been studied extensively for their interactions with clay.[10−14] The morphologies observed for these composites show both the exfoliated and intercalated structures that are now well-known for a number of other polymer/clay systems. The size and loadings of clay particles and their morphologies within the organic matrixes influence composite properties; the thermomechanical properties of PVOH, for example, have been shown to increase or decrease with clay loadings, depending on preparation conditions employed. The glass transition temperature (T_g), which reflects the relaxation dynamics of the polymer chains within a system, has been shown to be especially sensitive to structure within polymer/clay composites.[10−14] The relaxation dynamics, and hence T_g, are a length scale effect based on the cooperative rearranging region (CRR) length, defined as the minimum size region within which polymer chains must rearrange to render a blocked chain mobile. There is now substantial evidence that the origin of T_g nanoconfinement is related to surfaces and interfaces, which modify dynamics in the glass-forming regions.[15−18] Confinement of polymer between heterogeneous surfaces and interfaces at a length scale on the order of 100 nm has been shown to affect polymer glass transitions relative to their bulk values.[15] Within the 100 nm zone of confinement, different T_g values are observed, depending on whether a polymer chain is adsorbed to the surface of a reinforcing particle, located within the polymer bulk, or positioned on a air surface of the composite.

Given that levels of clays added and the nature of dispersion these clays within polymer matrixes are known to have major effects upon polymer relaxation dynamics, converting these same clays into clay aerogels and then into aerogel/polymer composites raises interesting new fundamental questions and provides a unique opportunity to further examine the concepts of polymer chain confinement. Clay aerogel/polymer and clay/polymer composites present significantly different bulk densities and free volumes; a comparison of chemically identical composite systems possessing different length scales of confinement is considered in the present work.

* Corresponding author. E-mail: das44@cwru.edu.

10.1021/ma0611826 CCC: $33.50
Published on Web 08/22/2006

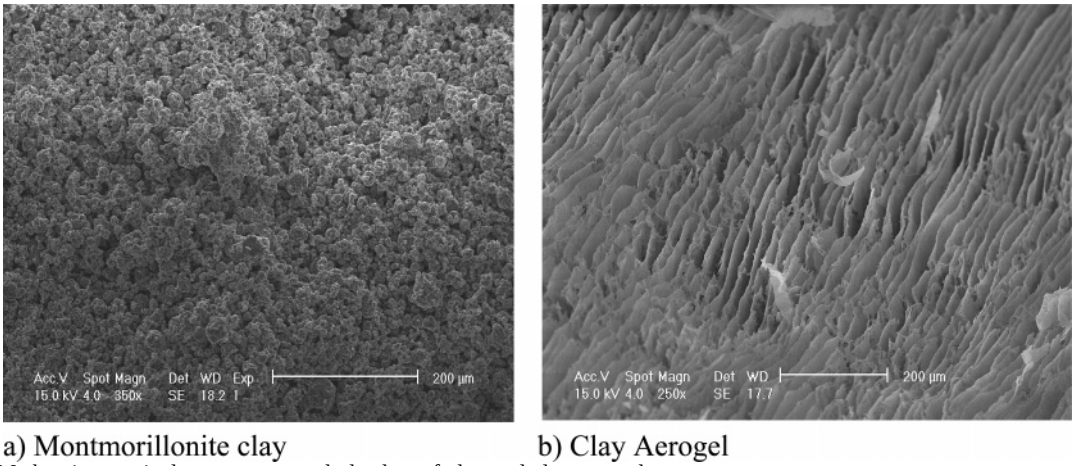

Figure 1. SEM showing particulate structure and platelets of clay and clay aerogel.

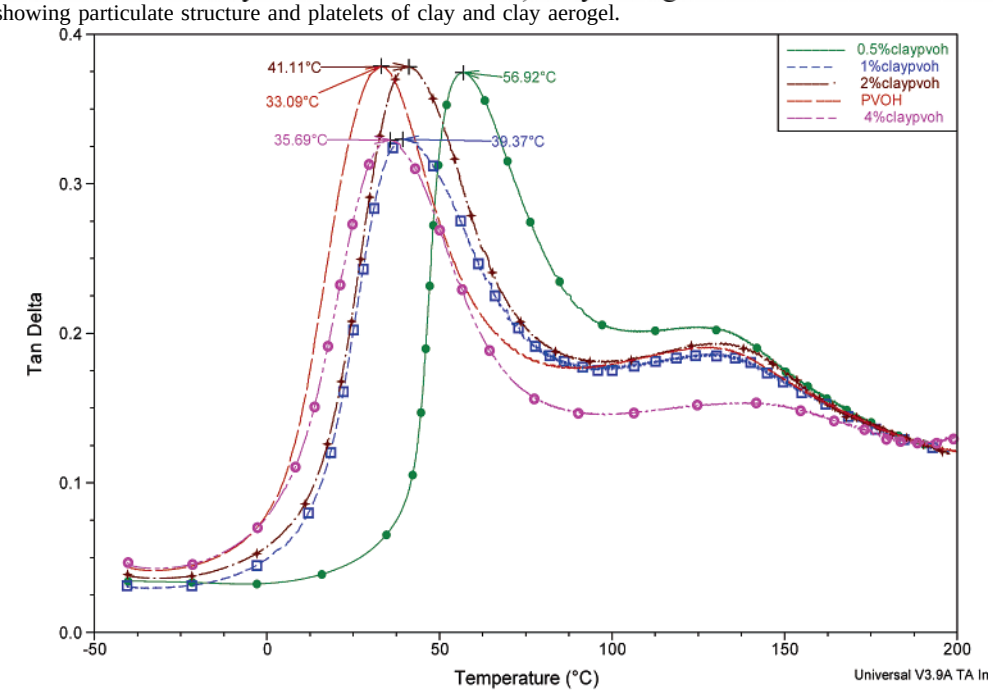

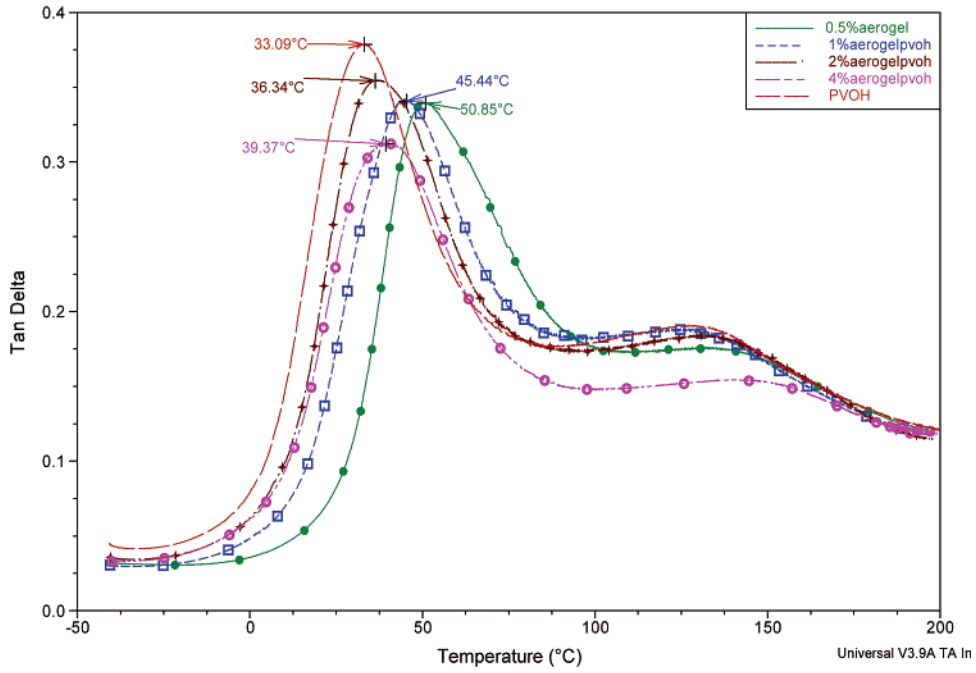

Figure 2. DMA spectra of "ambient" (a) PVOH/clay composites and (b) PVOH/aerogel composites.

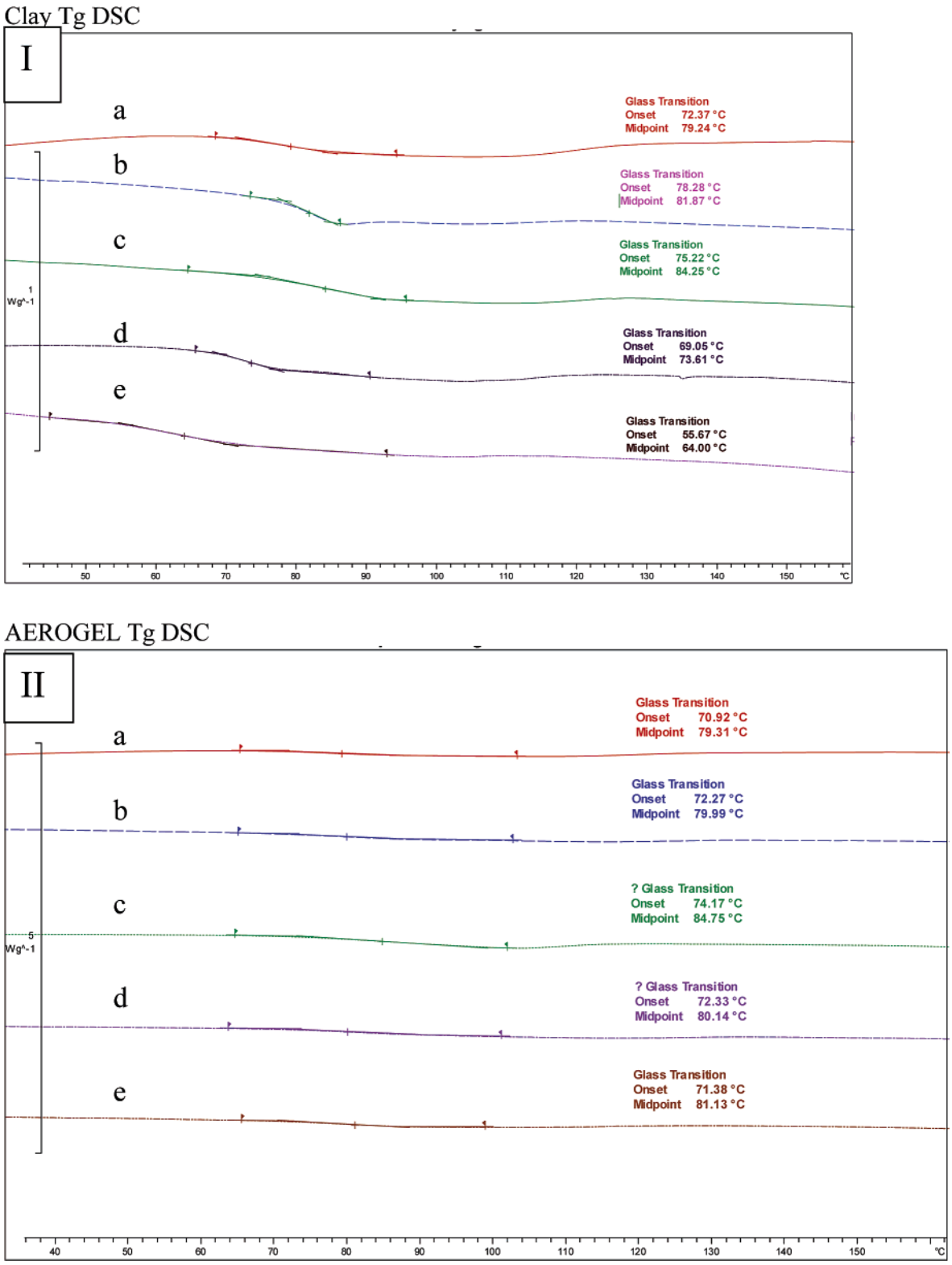

Figure 3. DSC spectra of "dry" (I) PVOH/clay composites a−e (PVOH control, C0.5, C1, C2, and C4) and (II) PVOH/aerogel composites a−e (PVOH control A0.5, A1, A2, and A4).

Experimental Section

Materials. Sodium-exchanged montmorillonite (PGW grade, MMT), with a cation exchange capacity (CEC) = 110 mequiv/100 g clay (MEQV), was supplied by Nanocor Inc. Poly(vinyl alcohol) (M_n = 108 kg/mol, 99.7% hydrolyzed) was purchased from Polyscience Inc.

Conversion of Clay to Clay Aerogel. A robust process for converting layered clays into clay aerogels was recently reported.[8] In a typical aerogel preparation, 4 g of clay was dispersed in 100 mL of water and sheared at high speed using a mechanical blender (Waring), and then the resulting clay gel was frozen within a cylindrical shell freezer using liquid nitrogen. Once frozen, the shell was attached to a (Virtis Freeze Mobile 35EL) freeze-drier maintained at −35 °C, and the ice was sublimed under vacuum to generate the aerogel. The conversion of clay to clay aerogel monoliths decreases its bulk density from 2.35 to ∼0.05 g/cm^3 and changes its morphology to that shown in Figure 1.

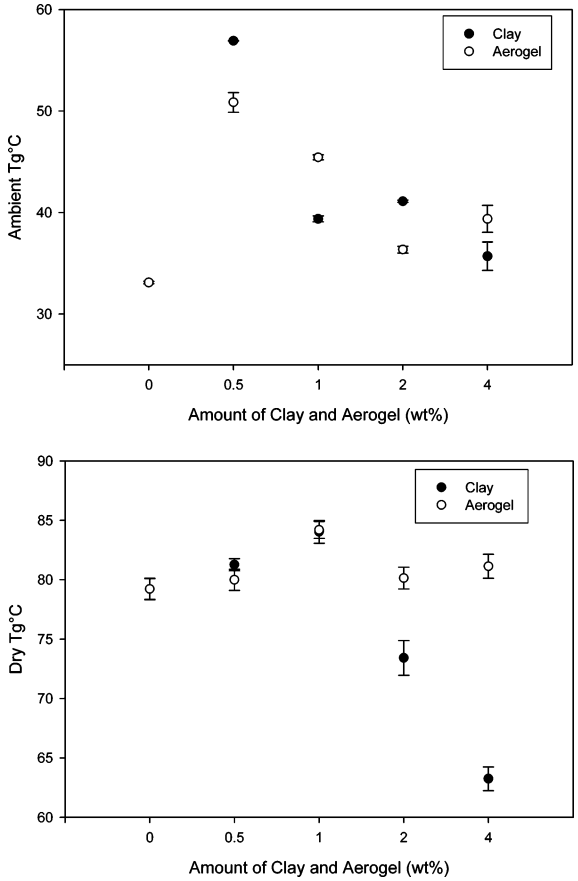

Figure 4. (a) Trend in "ambient" T_g (DMA). (b) Trend in "dry" T_g (DSC).

Synthesis of Clay and Clay Aerogel Composites. Both MMT clay and clay aerogel were dispersed in water for 1 h. In separate experiments, 0.5, 1, 2, and 4 wt % clay and clay aerogel dispersions were created, and then 10 wt % PVOH powder was added to these dispersions at 90 °C with vigorous stirring until optically clear (by eye) aqueous solutions were obtained. Films were cast from MMT/polymer dispersion onto smooth glass surfaces. The films were designated as A0.5, A1, A2, A4 and C0.5, C1, C2, C4 for aerogel and clay composites, respectively. Film thicknesses were controlled at 1 mm using a doctor blade while spreading the viscous dispersions; the samples were dried at 80 °C under vacuum for 24 h.

Characterization. DMA experiments were performed on a Q 800 DMA from TA Instruments which is equipped with a film-tension clamp. Films used for this experiment were dried at room temperature for 24 h to preserve flexibility in the films for testing in tension clamp and will be referred as "ambient composites". E' and E'' were measured over a range of −50 to 200 °C at 2° C/min heating rate and 1 Hz constant frequency; the force constant was fixed at 0.01 N with a displacement preset to 30 μm. Rectangular film samples with length-to-width ratios greater than 6 (10 mm × 1.5 mm) and film thicknesses of 0.2 mm were used to present uniform strain in the films under tension. The maximum value of tan δ was assigned as the glass transition temperature, T_g, for the composite. A JEOL 400 EX was used for transmission electron microscopy (TEM) studies; samples were prepared using pieces of film from each (A1, A4, C1, and C4) composite and were cast in epoxy used as a matrix. Films were microtomed into (200 nm−1 μm) thick slices and placed on a copper grid and imaged with an accelerating voltage of 100 kV. X-ray diffraction (XRD) experiments were performed on Rigaku diffractometer (Cu Kα radiation $\lambda = 1.54$ Å) with scattering measured from $2\theta = 2°$ to 45°. Films of clay and aerogel composites were dried under vacuum for 24 h at 80 °C for removal of water; these composites will be referred as "dry composites" herein. The composite thermal behaviors were studied using differential scanning calorimetry (DSC; Mettler Toledo model DSC 700c) with a temperature range of 25−300 °C at a temperature ramp of 10 °C/min.

Results

Glass transition temperatures were determined for PVOH/clay and PVOH/clay aerogel composites under ambient and dry conditions using DMA (Figure 2) and DSC (Figure 3) techniques, respectively. For DMA, the films had to be flexible for testing under tension and were therefore dried then equilibrated at room temperature/humidity. (Without equilibration, the samples were too brittle for reproducible DMA testing.) For DSC samples, films were dried under vacuum at 80 °C and maintained in a dry state for testing. The DSC testing under thoroughly dry conditions were chosen to provide information on polymer/clay interactions in the absence of water plasticization. Ambient condition composite films show similar trends for clay and clay aerogel, as illustrated in Figure 4. Under both ambient and dry conditions at low filler concentrations, an increase in T_g is observed; T_g then decreases with increasing clay or clay aerogel content only under ambient conditions. Under dry conditions, measured by DSC, the aerogel does not show decreased T_g at filler levels above 1%, whereas the clay composite T_g values steadily decline at the higher clay concentrations. The T_g values for these composites show a maximum at 1 wt % clay and clay aerogel content; a similar trend in the T_g of PVOH composites as a function of added MMT was recently reported.[13] It should be noted that when MMT/PVOH composites are prepared by varying degree of hydrolysis of poly(vinyl acetate), a different trend for dried composite T_g values vs added clay filler has been reported by other authors.[12] It is safe to say then that processing of clay/polymer composites can play an important role in ultimate material structure, which in turn determines observable properties. Comparing DSC results for dried composites (Figure 3b), a drop in T_g of 17 °C was observed for the clay composite, whereas the corresponding drop in T_g of the aerogel composite was only 3 °C. X-ray diffraction patterns in Figures 5 and 6 show d spacing increases in between clay platelets through the shift in the 001 peak from 12.6 to 15.5 Å for clay and 13.9 to 15.9 Å for clay aerogel, which confirms the presence of polymer intercalation within the clay platelets in both clay and clay aerogel composites. Although XRD confirms the presence of intercalation, the broad nature of the peak and tailing at lower 2θ obscures interpretation of morphology. A more realistic picture of the varying morphology containing nano- (<2 nm), meso- (2−50 nm), and microscale (>50 nm) features (utilizing the nomenclature of zeolites other ordered solids) and of clay platelets in the polymer matrix is achieved through TEM, as shown in Figure 7. Comparing A1 and C1 from Figure 7a,b, both intercalated and exfoliated regions in C1 can be seen, whereas for A1 the structure is not exfoliated to any significant extent, and it is similar to that of the mesoscale material shown in Figure 1. The clay aerogel structure thus is not completely destroyed even after subjected to high shear and temperature in water; this surprising kinetic stability of clay aerogels in water was recently reported.[9] Increasing clay aerogel content from 1 to 4 wt % (samples A1 to A4), the resulting separation between clay aerogel layers is poor, and hence the dispersion in the polymer matrix which is evident from Figure 7c,d.

It is known from the literature that poly(vinyl alcohol) will adsorb on clay surfaces and that clay can act as a nucleating agent for the crystallization of PVOH.[19−24] Surface crystallization behavior in the current study is evident from generation of more defined rings at the clay polymer interface, as measured

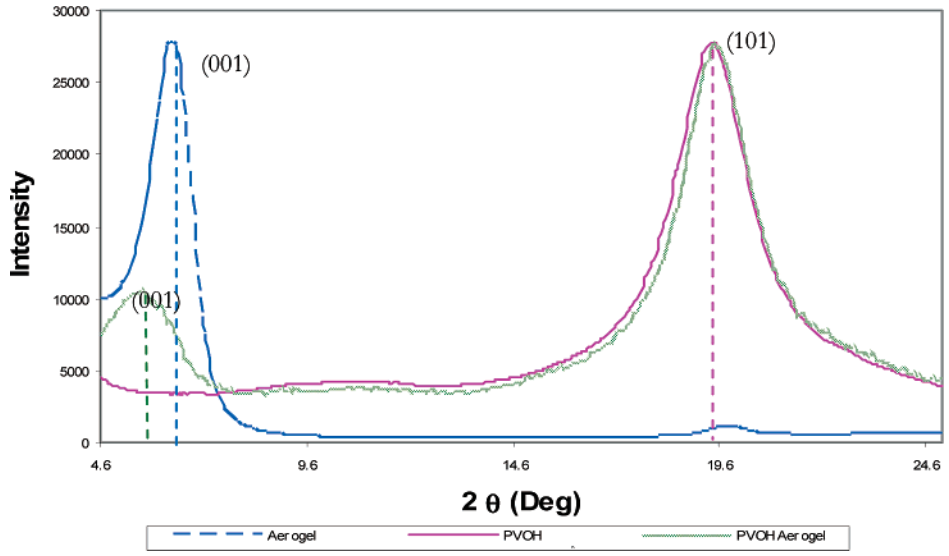

Figure 5. XRD of aerogel, PVOH, and PVOH/aerogel composites.

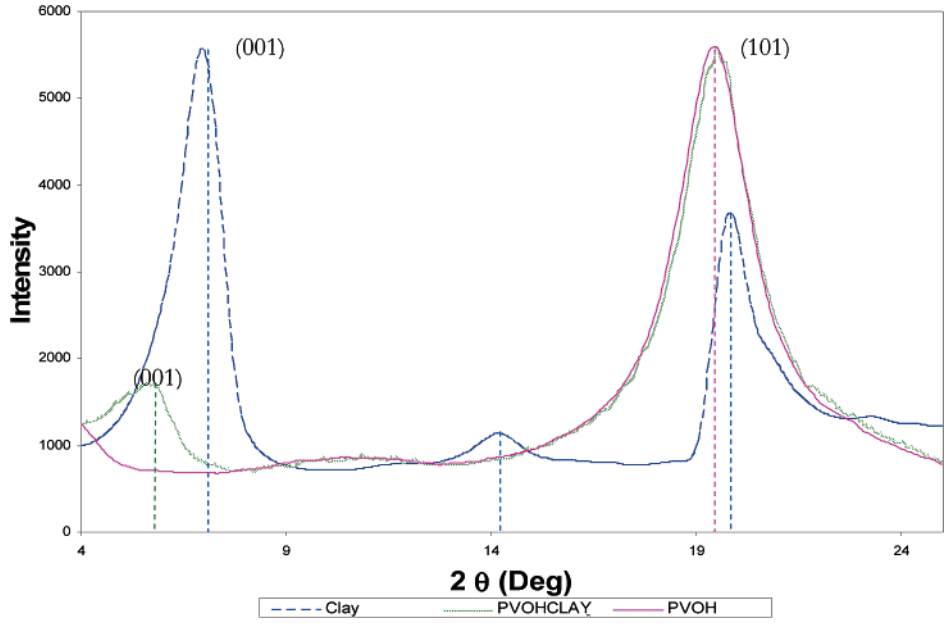

Figure 6. XRD of clay, PVOH, and clay/PVOH composites.

by in-situ TEM-XRD, as shown in Figure 8. The degree of crystallinity in these composites, due to the heterogeneous nucleation of clay and clay aerogels, was measured using DSC over the range 25−250 °C. The trend of bulk crystallization ΔH values measured at the peak centered at ∼223 °C for PVOH film. Clay and aerogel composites were compared against the experimental ΔH value (−62.8 J/g) of PVOH. Although the trend shows an overall decrease in ΔH values with increasing clay and clay aerogel content, the initial ΔH values for 0.5% and 1% are greater than the unfilled PVOH. The DSC scans in Figure 9 show the decreasing trend of bulk crystallinity with increasing clay aerogel content and the formation of another crystal phase presumably through surface-induced crystallization at higher loadings of the clay aerogel. The trend of ΔH from the clay aerogel composites in Figure 11 shows an abrupt change in ΔH value from A1 (−67.3 J/g) to a significantly lower value at A2 (−59.6 J/g). Further increasing the clay aerogel loadings from A2 to A4, the change in bulk crystallization is very small but is accompanied by an increase in the surface-induced crystallization peak at 245 °C. DSC scans in Figure 10 for clay composites show a decrease in their melting points and the development of a new crystal phase with increasing clay loadings. These behaviors are similar to those reported for solution-prepared PVOH/clay composites for greater than 2% clay content.[10] Although a decrease in the bulk crystallinity of clay composites of PVOH similar to that of aerogel is observed by DSC, clay composite does show an abrupt change with increase in clay content. Increasing levels of clay loading from C2 (−57.5 J/g) to C4 (−53.5 J/g), bulk crystals are reduced with increasing surface-induced crystallization peak at 235 °C.

Discussion

Polymer chains in the bulk have greater entanglement densities compared to those at interfaces.[25] As temperatures increase to values near T_g, long chain polymer molecules begin to disentangle and rearrange in a cooperative manner. The glass transition is associated with relaxation of cooperatively rearranging regions (CRR) of some tens to hundreds of repeat units of polymer chains, suggesting that the T_g is a length scale effect and extends up to 100 nm into the bulk.[15] In the clay composites studied herein, new clay−polymer interfaces are formed and will alter the entanglement density of the chains as well as the

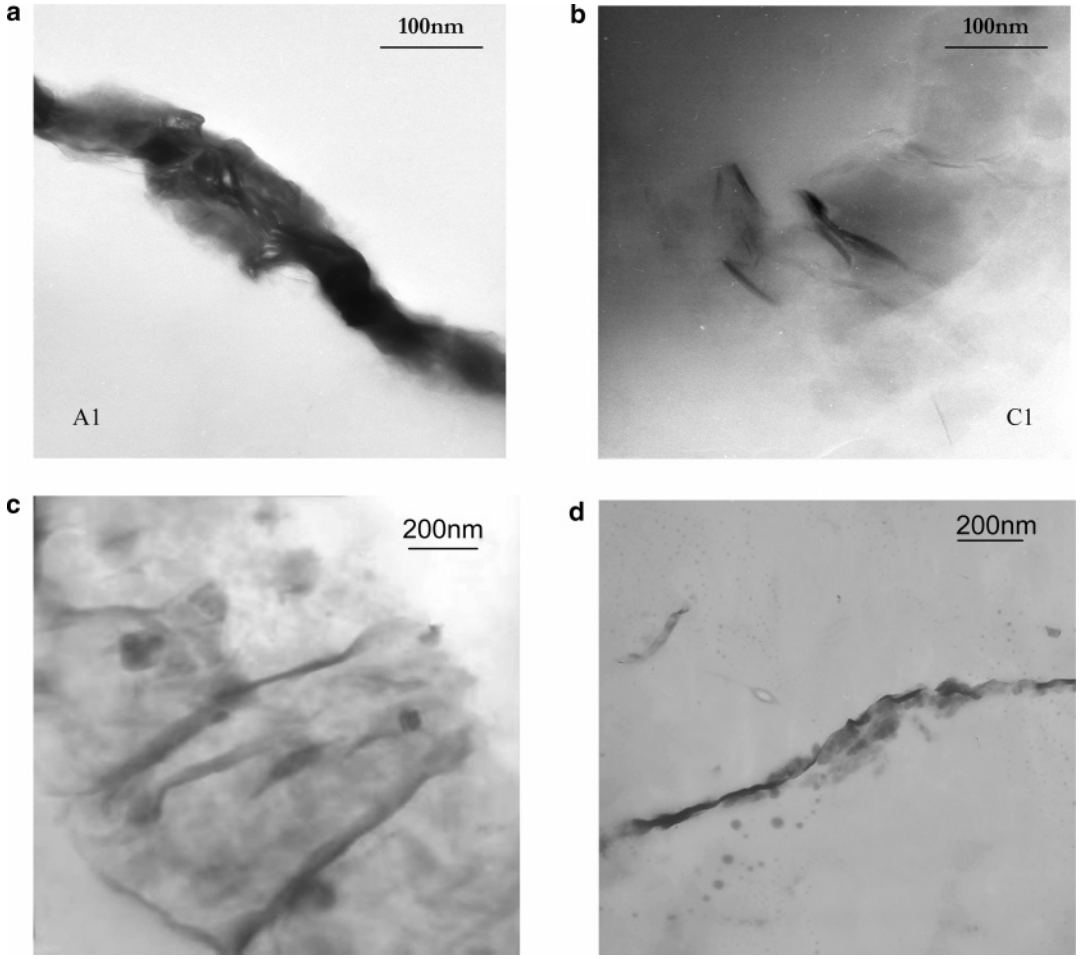

Figure 7. (a) PVOH with aerogel [A1]. (b) PVOH with clay [C1]. (c) PVOH with 4% aerogel [A4]. (d) PVOH with 1% aerogel [A1].

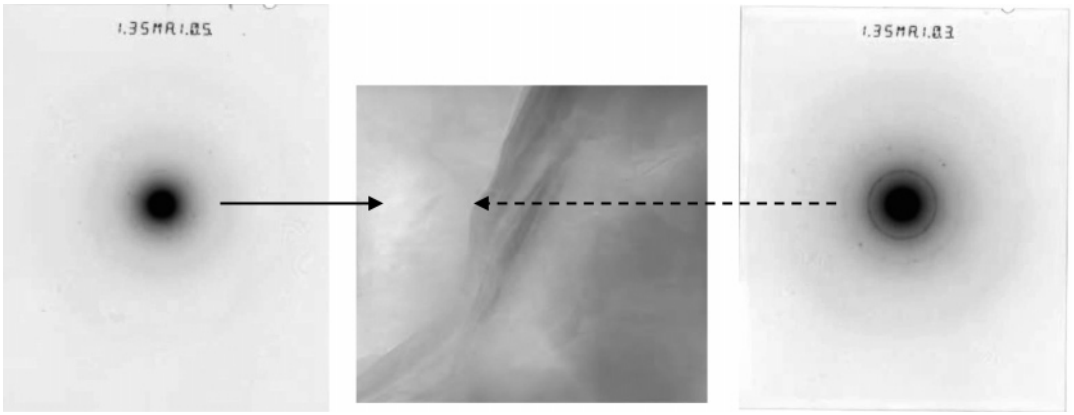

Figure 8. In-situ XRD pattern under TEM. The diffraction from the interphase shows more crystal reflection than in bulk.

length of cooperativity region, in turn greatly affecting the relaxation dynamics of polymer chains at these interfaces. The nature of interaction of polymers with the clay surfaces also will dictate the relaxation dynamics of the system. Polymer chains chemically grafted on the clay surface are expected to show lower relaxation rates compared to those of polymer chains physically adsorbed or hydrogen bonded to surfaces. Nonionic PVOH is thought to adsorb on the clay surfaces primarily through hydrogen bonding.[20,21] Both clay and clay aerogels, chemically identical but with different morphologies, contribute to the development of nano-, meso-, and microscale morphologies within polymer matrixes. Both increases and decreases of T_g have been reported for clay/polymer composites. Simple consideration of the configurational entropy theory of the glass transition[25,26] suggests that T_g should increase for polymer chains next to an impermeable surfaces due to restricted motion of polymer chains. On the contrary, free volume theories of the glass transition predict that a decrease in the density of polymer chains near clay−polymer interface due to increase in local free volume could cause a decrease in T_g.[27,28] Relaxation dynamics of polymer chains within the composite thus become a function of enhanced interaction with silicate layer and accelerated dynamics through an increase in local free volume near the clay−polymer interface.

The presence of impermeable surfaces in clay/PVOH composites leads to three dominant effects: (i) coupling of polymer chains to the surface through adsorption and hydrogen bonding which strengthen the interface (leads to an increase in T_g); (ii)

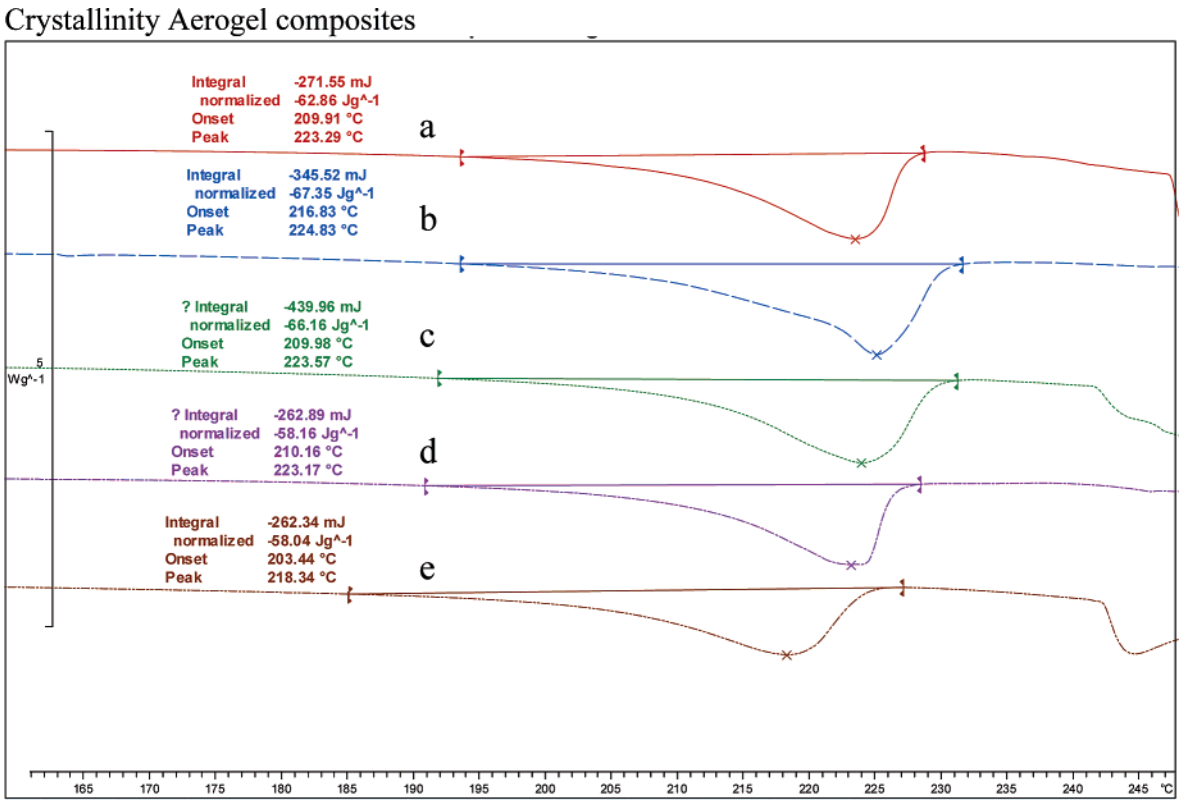

Figure 9. DSC of aerogel composites from a to e (PVOH control A0.5, A1, A2, and A4).

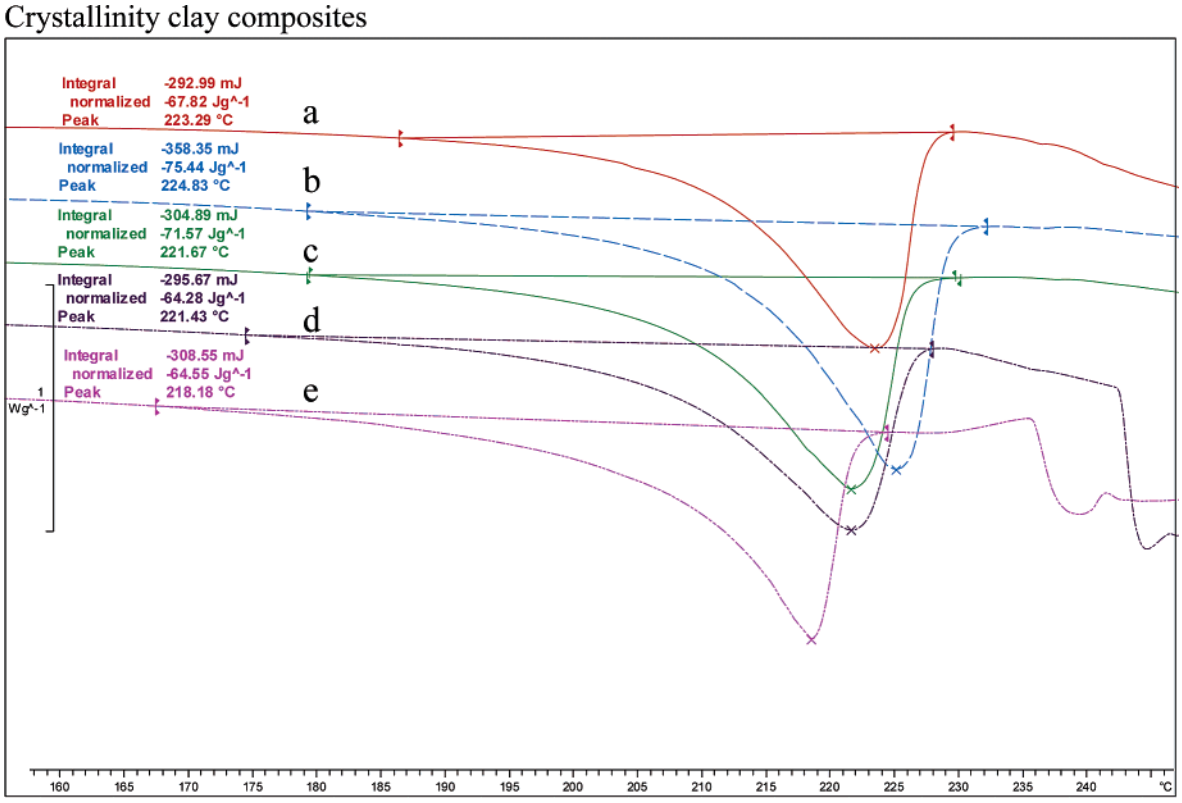

Figure 10. DSC of clay composites from a to e (PVOH control, C0.5, C1, C2, and C4).

extent of alignment of polymer chains between the clay platelets through intercalation (leads to a decrease in T_g); (iii) more rapid chain dynamics due to increase in local free volume at the clay−polymer interface (leads to a decrease in T_g). As all of the above effects are based on the size of interface, interfacial interactions play a dominant role in determining the net effect on T_g of clay composites. To explain how morphology and scale of dispersed clay affect composite properties, consider a matrix of polymer with clay and clay aerogel as shown in the Scheme 1. The morphologies and dispersions of clay and clay aerogel at 1 and 4 wt % shown below are comparable to TEM images given in Figure 7.

The characteristic length (CRR), ξ, is the region of minimum extent in which chains must rearrange to make a blocked chain

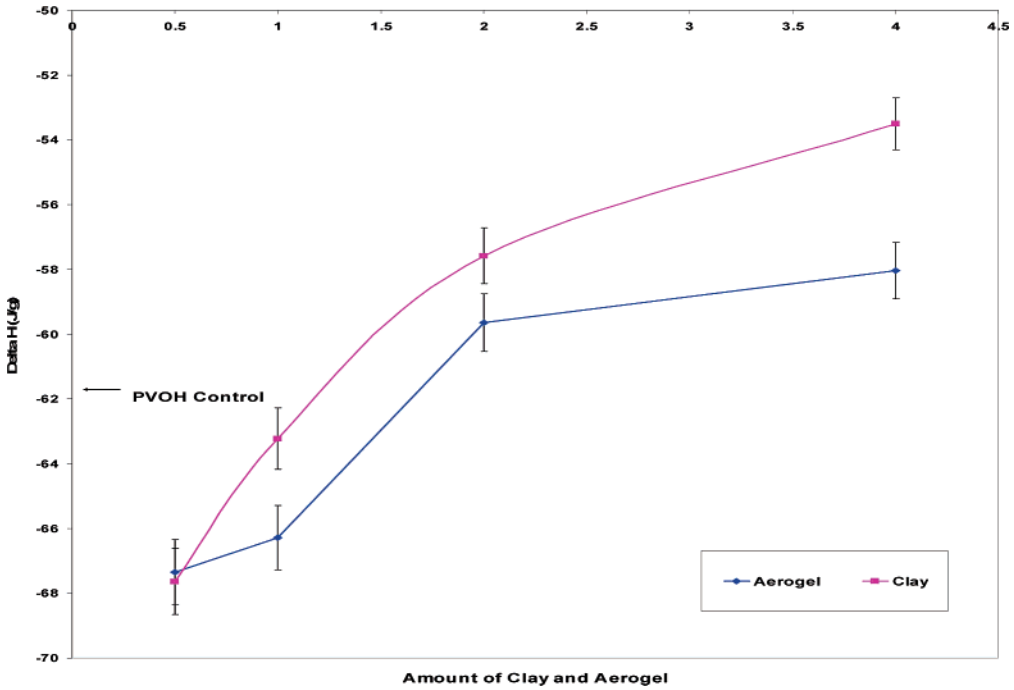

Figure 11. Trend in enthalpy of melting (ΔH) for clay composites.

Scheme 1. (a) Clay in Polymer Matrix; (b) Clay Aerogel in Polymer Matrix

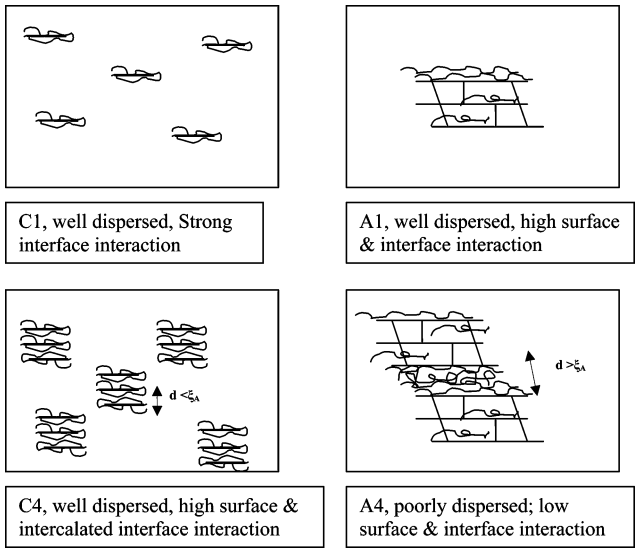

mobile. If the interlayer spacing between clay sheets is less than the length of a characteristic length of CRR ($d < \xi$), which generally extends in the range of 1.3−3 nm, the intercalated polymer shows a confinement effect and hence greater chain dynamics.[29,30] Clay inherently has a very high specific surface area (over 700 m^2/g in its exfoliated state), presenting a high interfacial area to interact with polymer.[24] In the case of exfoliated clay composites with greater interfacial area as in C1, favorable interactions between polymer and the clay surfaces are dominant and lead to reduced relaxation dynamics, which results in higher T_g. At higher clay loadings both interfacial area and intercalation are enhanced as shown for C4 and is also evident from XRD and TEM. The polymer chains are then confined between the clay sheets whose distance ($d < \xi$) becomes comparable to effective CRR of the polymer and are subjected to a confinement effect. Under confinement the molecules inside the clay sheets are aligned mechanically, resulting from fewer entanglements and bringing about enhanced relaxation dynamics within the composite. Because of the presence of heterogeneous clay in the PVOH matrix, the local free volume is also enhanced at the interface which results in greater relaxation dynamics of the polymer chains and lowers its T_g value. In the case of the aerogel (A1) composite, in Figure 7a, a single large surface for interaction is presented to the polymer. Favorable interaction between polymer and clay aerogel surface results in low relaxation dynamics and hence higher T_g. At higher loading of clay aerogel as in A4, there is an overall decrease in dispersion, and thus the interfacial area for interaction with the polymer is reduced. The separation between the clay aerogel layers is greater than the length of CRR ($\xi > d$), at which the confinement effect is not dominant. Thus, surface effects dominate the resulting properties of the composites. The trend of T_g decline (Figure 4b) suggests the effect on T_g for the clay composite at higher clay loading is dramatic compared to the T_g of clay aerogel composite.

The observed trend in T_g for both clay and clay aerogel composites can also be correlated to the trend in bulk crystallinity measured at 223 °C. Overall increases in crystallinity of the composite are observed due to surface-induced crystallization (Figure 11). An increase in the crystalline fraction decreases the amorphous fraction and hence lowers the free volume at the interface. At low concentrations of clay and clay aerogel, large interfacial areas provide effective locations for surface nucleation, and hence the overall crystallinity is greater than the bulk. Thus, T_g increases with higher crystalline fraction. At higher loadings of clay aerogel, poor dispersion/disruption of the interconnected multiple layers specifically results in surface-induced crystallization of polymer chains on the large clay surface and simple insertion of polymer within internal aerogel "supergalleries"; this is evident from the limited decrease in bulk ΔH value from A1 to A4 closer to ΔH value of bulk polymer along with increasing peak at 245 °C. Because of the poor dispersion of individual clay aerogel layers in the PVOH matrix, the localized increase in surface-induced crystals does not affect the bulk relaxation process, and hence T_g values at higher clay aerogel content are closer to the T_g of the bulk. Although the trend for clay composites is similar to that of clay

aerogel, the T_g of the composite with increasing clay content is lower than the bulk T_g of PVOH; this is likely due to the better dispersion of the clay within the polymer matrix, uniformly lowering the bulk crystalline fraction and generating greater overall free volume in the composite.

Conclusions

Chemically identical clay and clay aerogels with varying morphologies and length scales, when dispersed within an interacting polymer such as PVOH, exhibit markedly different behaviors. The trend in T_g values within these composites is explained by surface-induced crystallization and free volume of the polymer in this morphology. The relative increase or decrease in T_g is proposed to be determined by two competing effects: (i) surface interaction which strengthens the interface decreasing chain mobility and (ii) enhanced interfacial free volume due to lower crystallinity of polymer chains which increases chain mobility. Thus, relaxation dynamics of a polymer chain, which is a length-scale effect, is dependent on the size scale (nano or meso) of heterogeneous clay, its morphology, and dispersion in the polymer matrix. The presence of clay or clay aerogels within the polymer enhances interfacial interactions due to effective surface nucleation at low concentrations and increases free volume at higher concentrations, thus reducing the polymer−polymer bulk interactions. Differences in T_g values at nanoscale clay composites are significantly higher than mesoscale clay aerogel composites and can be attributed to effective localized surface area for interaction with the polymer.

References and Notes

(1) Alexandre, M.; Dubois, P. *Mater. Sci. Eng.* **2000**, *28*, 1−63.
(2) Van Olphen, H. *Clay Mineral.* **1967**, *15*, 423−435.
(3) Mackenzie, R. C. *Nature (London)* **1952**, *171*, 682.
(4) Call, F. *Nature (London)* **1953**, *172*, 126.
(5) Weiss, A.; Fahn, R.; Hofmann, U. *Naturwissenschaften* **1952**, *39*, 351−2.
(6) Norrish, K.; Russell-Colon, J. A. *Clay Mineral. Bull.* **1962**, *5*, 9−16.
(7) Nakazawa, H.; Yamada, H.; Fujita, T.; Ito, Y. *Clay Sci.* **1987**, *6*, 269−76.
(8) Somlai, L. S.; Bandi, S. A.; Mathias, L. J.; Schiraldi, D. A. *AIChE J.* **2006**, *52*, 1162−1168.
(9) Bandi, S. A.; Bell, M.; Schiraldi, D. A. *Macromolecules* **2005**, *38*, 9216−9220.
(10) Strawhecker, K. E.; Manias E. *Chem. Mater.* **2000**, *12*, 2943−2949.
(11) Strawhecker, K. E.; Manias, E. *Macromolecules* **2001**, *34*, 8475−8482.
(12) Grunlan, J.; Grigorian, A.; Hamilton, C.; Mehrabi, A. *J. Appl. Polym. Sci.* **2004**, *93*, 1102−1109.
(13) Ogata, N.; Kawakage, S.; Ogihara, T. *J. Appl. Polym. Sci.* **1997**, *66*, 573−581.
(14) Strawhecker, K. E.; Manias, E. *J. Chem. Phys.* **2003**, *118*, 3421−3429.
(15) Priestly, R. D.; Ellison, C. J.; Broadbelt, L. J.; Torkelson, J. M. *Science* **2005**, *309*, 456−459.
(16) Manias, E.; Kuppa, V.; Yang, B.; Zax, D. B. *Colloids Surf., A* **2001**, *187−188*, 509−521.
(17) Tran, T.; Grohens, S. *Composites: Part A* **2005**, *36*, 461−465.
(18) Rault, J. *J. Macromol. Sci., Part B: Phys.* **2003**, *B42*, 1235−1247.
(19) Pattanayek, S. K.; Juvekar, V. A. *Macromolecules* **2002**, *35*, 9574−9585.
(20) De Bussetti, S. G.; Ferreiro, E. A. *Clays Clay Miner.* **2004**, *52*, 334−340.
(21) Chang, J. H.; Jang, T. G.; Ihn, K. J.; Lee, W. K.; Sur, G. S. *J. Appl. Polym. Sci.* **2003**, *90*, 3208−3214.
(22) Isci, S.; Gunistera, E.; Ece, O. I.; Gungor, N. *Mater. Lett.* **2004**, *58*, 1975−1978.
(23) Assender, H. E.; Windle, A. H. *Polymer* **1998**, *39*, 4295−4302.
(24) Carrado, K. A.; Thiyagarajan, P.; Elder, D. L. *Clays Clay Miner.* **1996**, *44*, 506−514.
(25) Brown, H. R.; Russell, T. P. *Macromolecules* **1996**, *29*, 798−800.
(26) Gibbs, J. H.; DiMarzio, E. A. *J. Chem. Phys.* **1958**, *28*, 373−83.
(27) Gibbs, J. H.; DiMarzio, E. A. *J. Chem. Phys.* **1958**, *28*, 807−13.
(28) Jackson, C. L.; McKenna, G. B. *J. Non-Cryst. Solids* **1991**, *221*, 131−133.
(29) Jackson, C. L.; McKenna, G. B. *Chem. Mater.* **1996**, *8*, 2128−37.
(30) Alcoutlabi, M.; McKenna, G. B. *J. Phys.: Condens. Matter* **2005**, *17* R461−R524.

MA0611826